FIGURE S1

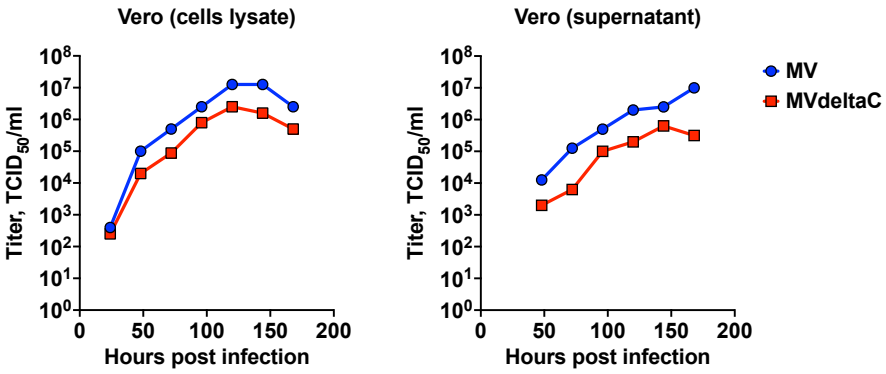

Figure S1. Growth kinetics of MV and MVdeltaC on Vero cells. Cells were infected at MOI 0.01 and incubated at 32°C. The data show reciprocal endpoint dilution titers of cell-associated (left) and cell-free (right) viruses.

FIGURE S2

Figure S2. Sequencing analysis of MVdeltaC passages. Reads coverage and proportion of intrasample single nucleotide variants (iSNVs) obtained from next-generation sequencing of MVdeltaC at passages 5 (P5) and 10 (P10). A schematic of the measles virus genome is shown below using the same scale, with the two engineered mutations preventing C protein expression highlighted. No sequence changes were detected at either of these positions in P5 or P10 samples.

FIGURE S3

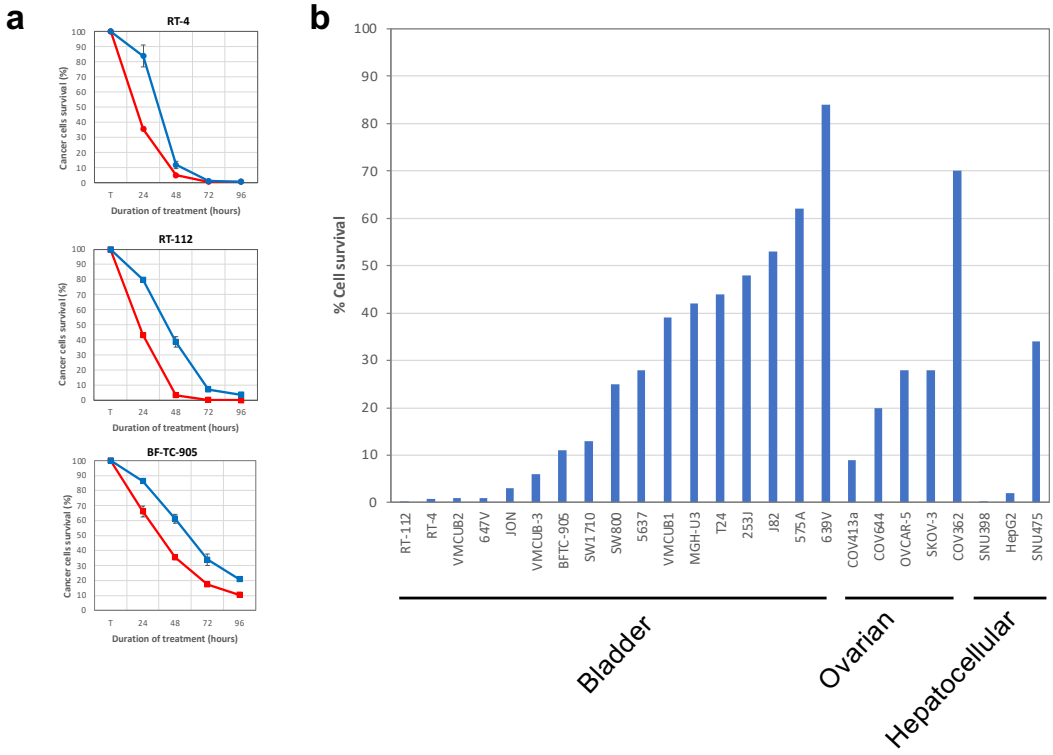

Figure S3. Infection and killing of human cancer cells by MVdeltaC. (a) Cell survival of three human bladder cancer cell lines after infection with MV (blue) or MVdeltaC (red) at MOI 5, measured by CellTiter-Glo assay; means ± SD; measurements are in triplicate; data normalized to non-infected cells. (b) MVdeltaC killing of a series of human cancer cells of bladder, ovarian or hepatocellular origin as determined by CellTiterGlo assay (cancer cells survival after 72 hours of infection at MOI 5).

FIGURE S4

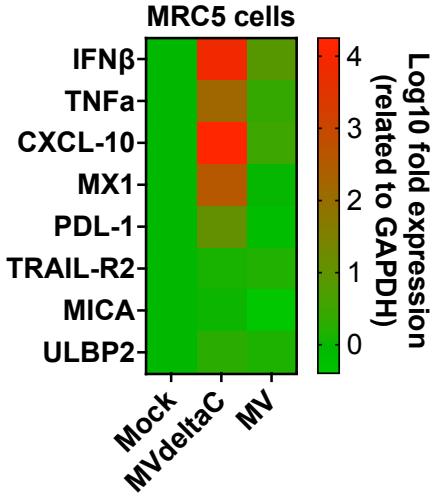

Figure S4. Gene expression analysis in infected MRC5 cells. Heatmap of differentially expressed genes in MRC5 cells after 24h incubation with MV, MVdeltaC (MOI 1) or PBS (Mock); experiment in triplicate, a gradient of colors from green to red represent $\log_{10}$ fold change values from lowest to highest, respectively.

FIGURE S5

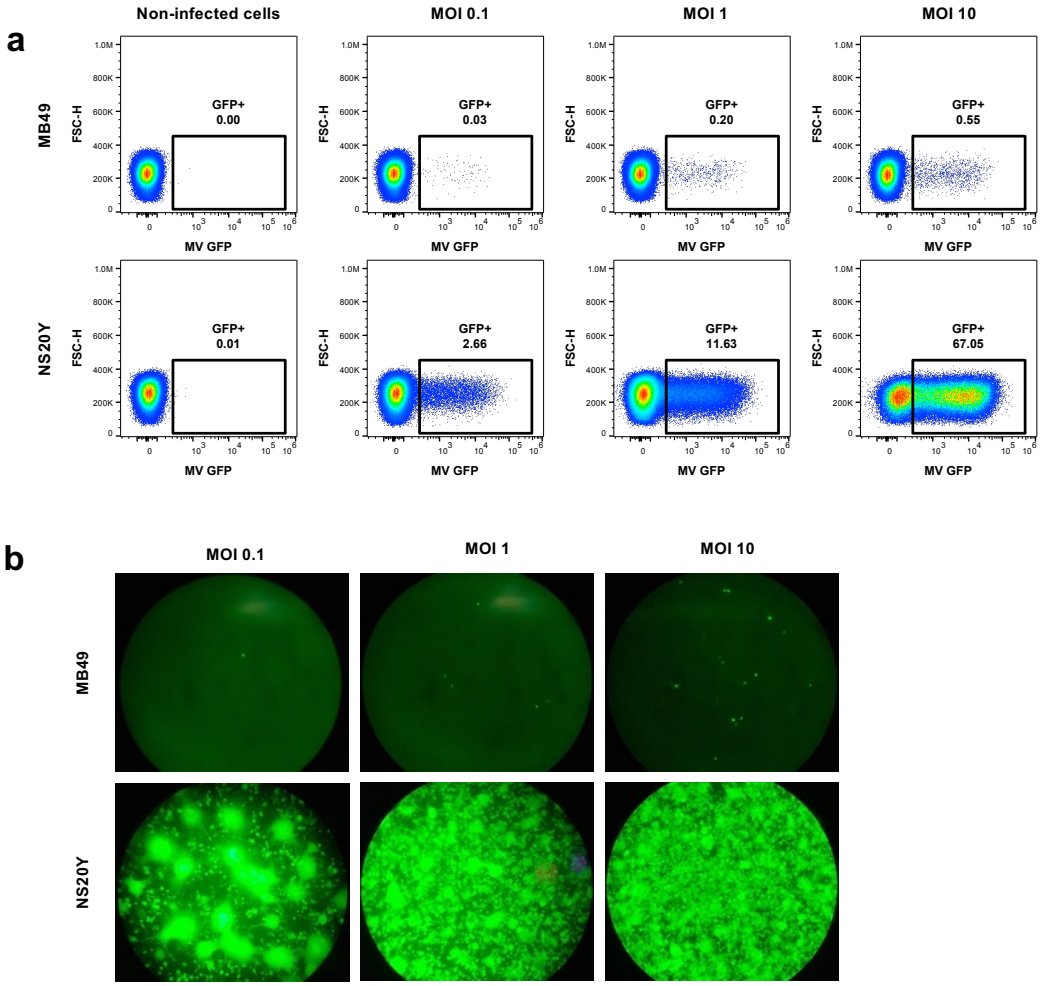

Figure S5. NS20Y cells are permissive to measles infection. Mouse neuroblastoma NS20Y cells and bladder carcinoma MB49 cells were infected with MV-eGFP at the indicated MOI and analyzed by (a) flow cytometry 24 hours post-infection, and (b) immunofluorescence microscopy 72 h hours post-infection.

FIGURE S6

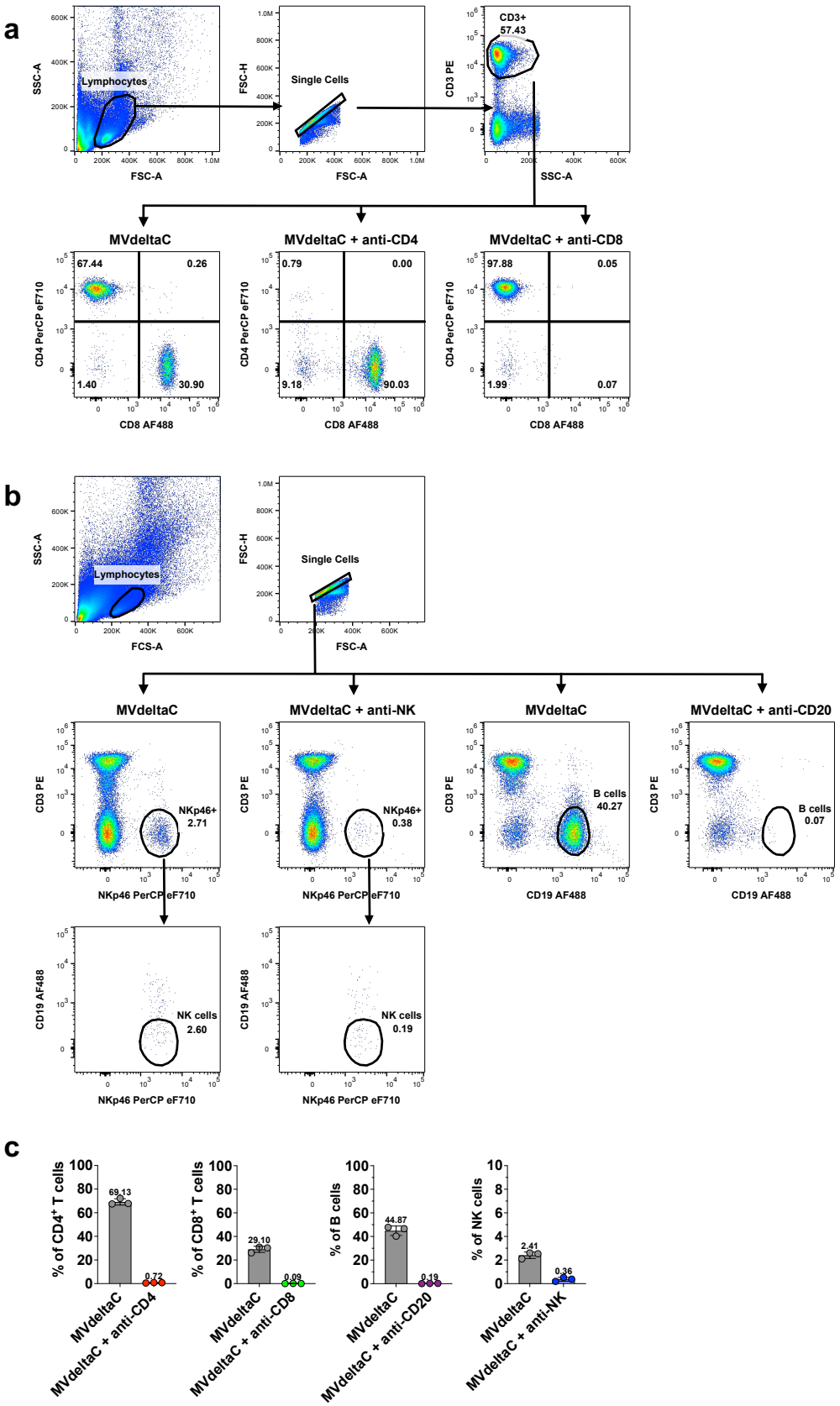

Figure S6. Flow cytometry analysis of immune cell populations in the blood of A/J mice depleted for CD4$^+$, CD8$^+$, B or NK cells. (a) Representative dot plots show the flow cytometry gating strategy to identify CD4$^+$ (CD3$^+$ CD4$^+$ CD8$^-$), CD8$^+$ (CD3$^+$ CD8$^+$ CD4$^-$) or (b) NK (CD3$^-$ NKp46$^+$ CD19$^-$) and B (CD3$^-$ CD19$^+$) cell populations in the blood of treated mice. Mice were grafted with 5x10^6 NS20Y murine tumor cells on day 0. T cell depletion was achieved by i.p. injection of anti-CD4 or anti-CD8 mAbs (200 µg in 100 µL of PBS) on days 5, 6 and 7 after NS20Y cells injection. NK or B cell depletion was performed on days 5 and 7 using 50µg of anti-asialo GM1 or 200µg of anti-CD20 antibodies, respectively. Sustained immune cell depletion was achieved by weekly antibody administrations on days 14 and 21. Tumor therapy with MVdeltaC at 2x10^{6}TCID$_{50}$ was performed on days 6, 9 and 12. Immune cell populations in the groups of A/J mice were analyzed on day 27. (c) Bar graphs show flow cytometry data for the three animals from each group, means ± SD.

FIGURE S7

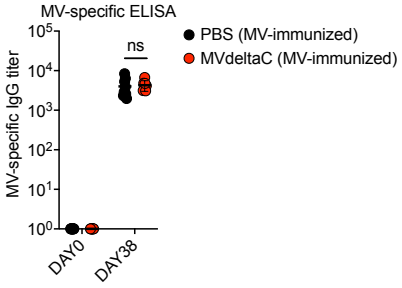

Figure S7. MV-specific IgG antibody responses in A/J mice following MV Schwarz vaccination. Mice were immunized i.p. with MV Schwarz (1×10^5 $TCID_{50}$) on day 0. Sera were collected at day 38 post-immunization and assessed for IgG antibody responses to MV antigens by ELISA. The data show the reciprocal endpoint dilution titers of MV-specific IgG antibodies in preimmune (day 0) and day 38 sera; each point represents an individual mouse; means ± SD, n= 7-9 per group; unpaired two-tailed t test; ns, not significant.

FIGURE S8

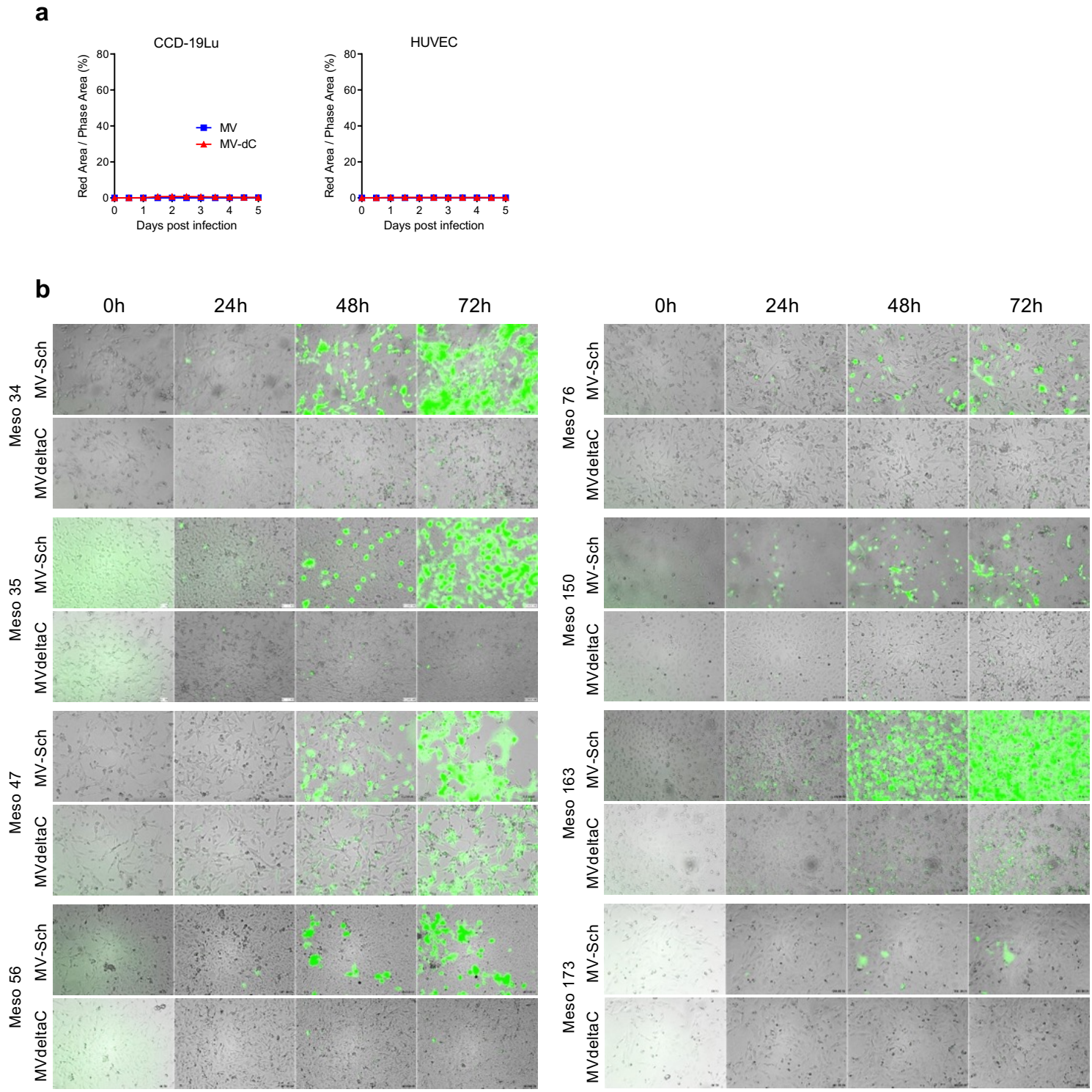

Figure S8. Infection of healthy and cancer human cells by MV or MVdeltaC. (a) Quantification of virus propagation in healthy lung fibroblasts (CCD19-Lu) or endothelial cells (HUVECs) infected with either MV-mCherry or MVdeltaC-mCherry. (b) Time-lapse microscopy analysis of mesothelioma cell lines infected with MV-eGFP or MVdeltaC-eGFP (MOI = 1).

FIGURE S9

VIDEOS MESO13

Figure S9. Infection of Meso 13 mesothelioma cells by MV or MVdeltaC.
Time-lapse microscopy analysis of mesothelioma cell lines infected with MV-eGFP (a) or MVdeltaC-eGFP (b) (MOI = 1).

FIGURE S10

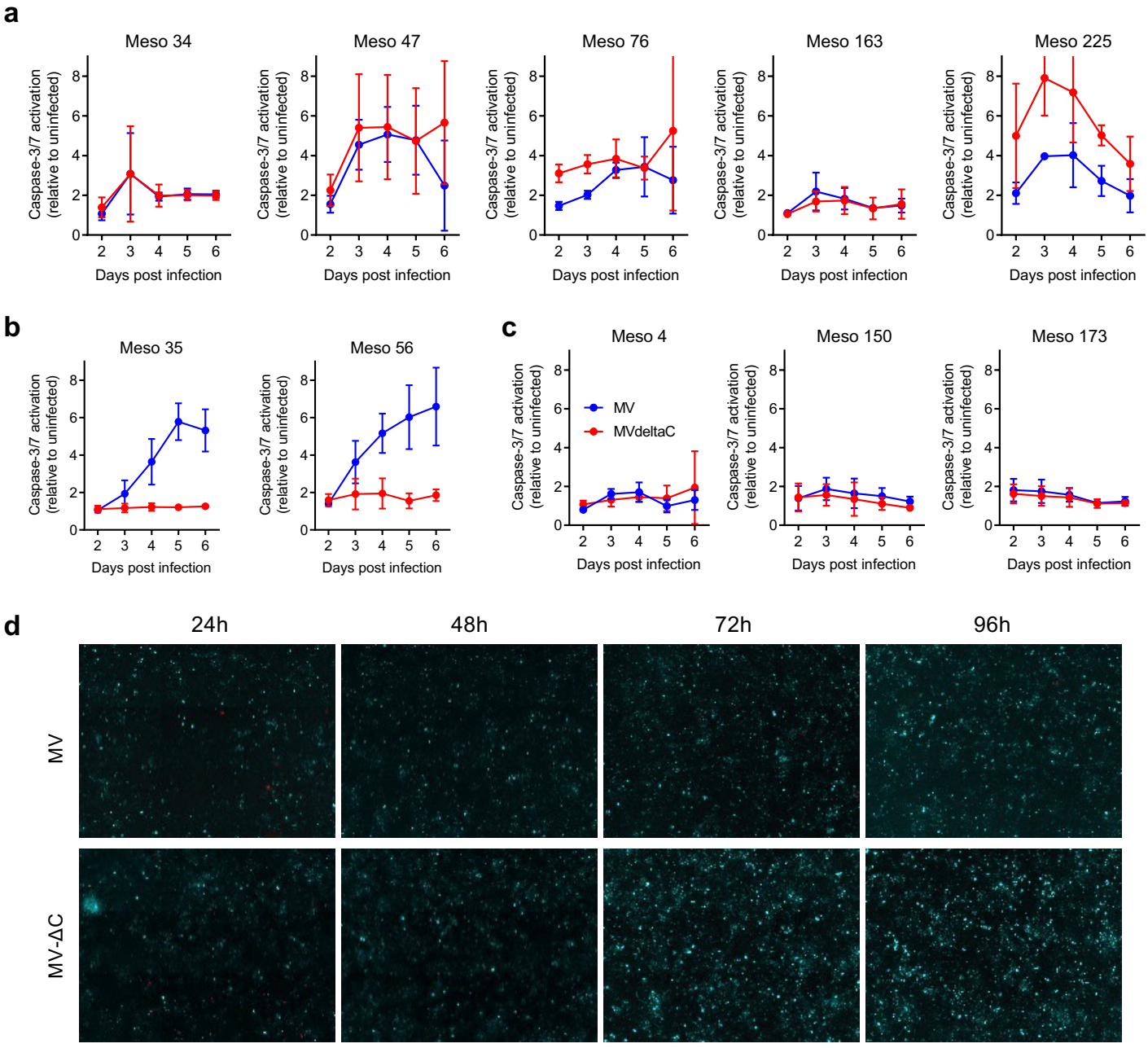

Figure S10. Activation of Caspases-3/7 in mesothelioma cells infected by MVdeltaC. (a-c) Luminescence-based quantification of caspase-3/7 activity in human mesothelioma cell lines. (a) MV-permissive, (b) MVdeltaC-resistant, and (c) MV-resistant cells. (d) Fluorescence microscopy of Meso 4 cells showing caspase-3/7 activation (cyan) after infection with MV-mCherry or MVdeltaC-mCherry (red).

FIGURE S11

a

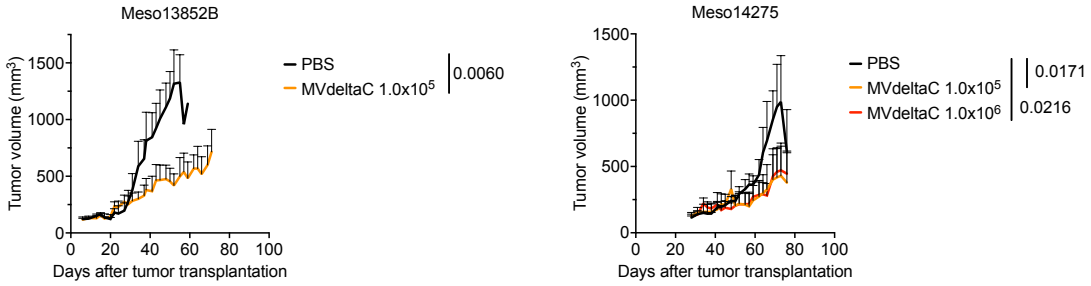

Figure S11. MVdeltaC inhibits human PDX growth in immunodeficient mice. Growth of mesothelioma PDX tumors in NMRI nu/nu mice after weekly MVdeltaC therapy at two doses; means ± SEM, n = 3 mice per group; each group was compared to PBS group (unpaired one-tailed t test).

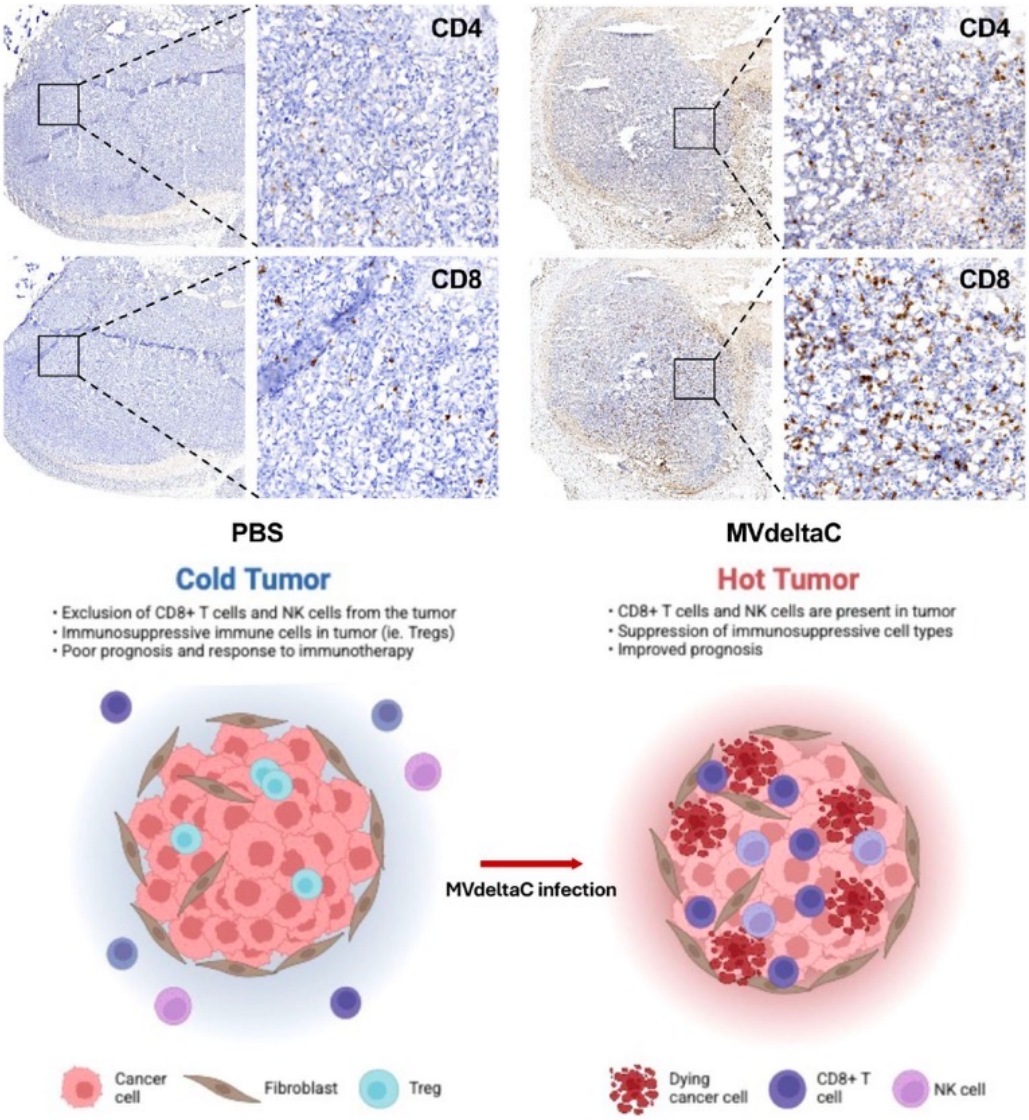
CD4
CD8
CD4
CD8
PBS
MVdeltaC
Cold Tumor
• Exclusion of CD8+ T cells and NK cells from the tumor
• Immunosuppressive immune cells in tumor (ie. Tregs)
• Poor prognosis and response to immunotherapy
Hot Tumor
• CD8+ T cells and NK cells are present in tumor
• Suppression of immunosuppressive cell types
• Improved prognosis
MVdeltaC infection
Cancer cell
Fibroblast
Treg
Dying cancer cell
CD8+ T cell
NK cell